Turkish Journal of Electrical Engineering and Computer Sciences

Volume 26 | Number 6 Article 19

1-1-2018

A matched E-H plane T-junction for X-band applications

ASHMI CHAKRABORTY DAS

SANTANU DWARI

AMIT BAGE

Turkish Journal of Electrical Engineering & Computer Sciences

http://journals.tubitak.gov.tr/elektrik/

Research Article

Turk J Elec Eng & Comp Sci
(2018) 26: 3007 – 3023

doi:10.3906/elk-1704-237

A matched E-H plane T-junction for X-band applications

Ashmi CHAKRABORTY DAS[1], **Santanu DWARI**[1], **Amit BAGE**[2,*]

[1]Department of Electronics Engineering, Indian Institute of Technology (Indian School of Mines), Dhanbad, Jharkhand, India

[2]Department of Electronics and Communication Engineering, SRM Institute of Science and Technology, Kattankulathur, Chennai, Tamil Nadu, India

Received: 20.04.2017 • **Accepted/Published Online:** 03.04.2018 • **Final Version:** 29.11.2018

Abstract: This paper presents a method of moment-based analysis of an E-H plane T-junction to find its scattering parameters. The results show that the network is not matched at its ports. Therefore, matching networks have been included in the structure to establish matching at the ports. The matching structure includes an inductive window at the H-plane arm and a bisected funnel structure at the junction. Results of the modified structure show simultaneous matching at all the four ports at 9 GHz, which makes it suitable for X-band application.

Key words: E-H plane T-junction, matching network, iris, scattering parameter

1. Introduction

E-H plane T-junctions are the building blocks of the monopulse comparator circuits of monopulse radar. The circuit is used to route the transmitting pulse towards the antennas as well as to process and analyze the echo signals to find azimuth and elevation errors. Therefore, the E-H plane T-junctions must be matched at all its ports. E-H plane T-junctions are also used in microwave systems to measure unknown impedance, to double the feed power of an antenna, as duplexers, to build four-port circulators, as E-H tuners, and as mixers.

Due to various applications in wireless and microwave measurement systems, E-H planes T-junctions were analyzed by different researchers at different times. Sieverding and Arndt [1] used a mode-matching technique to find the S-matrix of an E-H plane T-junction. However, the junction was not matched at its ports. Ritter and Arndt [2] presented a combined finite difference time domain (FDTD)-matrix pencil method for the calculation of S-parameters of a matched E-H plane T-junction. They used a stepped cylindrical stub at the junction and an inductive post at the E-plane arm to match the ports. However, simultaneous matching of all the ports was not achieved. Shen et al. [3] proposed a hybrid finite element-modal expansion method to analyze E-H plane T-junctions. They used an inductive window at the E-plane and a combination of conical and cylindrical stubs at the junction to match the ports, but again simultaneous matching of the ports was not achieved. Beyer and Rosenberg [4] designed an E-H plane T-junction using a stepped impedance post at the junction. Dou and Zhang [5] analyzed a forked E-H plane T-junction using the FDTD method. However, the structure did not incorporate any matching network and hence was not matched at its ports. Wu and Dou [6] used a mode expansion method and finite element method to analyze a W-band E-H plane T-junction. They used a truncated cone between two cylindrical posts at the junction to match the ports.

*Correspondence: bageism@gmail.com

The first section of this paper presents a method of moment-based analysis [7] of an E-H plane T-junction to find its scattering parameters. In the next section a matched E-H plane T-junction is presented. Matching has been obtained by using a symmetric inductive iris at the H-plane arm and a bisected funnel structure at the junction.

2. Analysis of E-H plane T-junction

To analyze the E-H plane T-junction, initially the circuit has been modeled in terms of multiple rectangular waveguide sections (or blocks), as shown in Figure 1. Next, using the equivalence principle, the common apertures between different blocks have been replaced by electric walls with equivalent magnetic currents. This transforms the individual blocks into cavities. The cavity modeling of the structure, with equivalent magnetic current densities at the apertures, is shown in Figure 2. It consists of four waveguide regions, W_1 through W_4 (representing the ports of the network); three cavity regions, C_1 through C_3; and eight interfacing apertures between them (carrying equivalent magnetic currents M_1 through M_8).

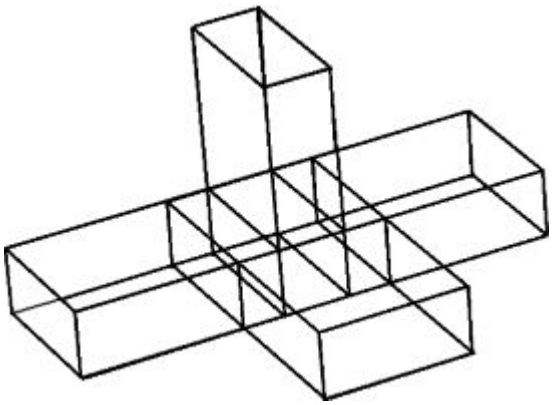

Figure 1. Modeling of E-H plane T-junction in terms of multiple waveguide sections/blocks/cavities.

Applying the continuity condition of the tangential components of aperture magnetic fields across the apertures, we get the following.

$$\begin{aligned} &H_x^{w(1)}(M_1^x) + H_x^{c(1)}(M_1^x) + H_x^{w(1)}(M_1^y) + H_x^{c(1)}(M_1^y) - H_x^{c(1)}(M_2^x) - H_x^{c(1)}(M_2^y) \\ &+H_x^{c(1)}(M_5^z) + H_x^{c(1)}(M_5^y) = 2H_x^{inc(1)} \end{aligned} \tag{1}$$

$$\begin{aligned} &H_y^{w(1)}(M_1^x) + H_y^{c(1)}(M_1^x) + H_y^{w(1)}(M_1^y) + H_y^{c(1)}(M_1^y) - H_y^{c(1)}(M_2^x) - H_y^{c(1)}(M_2^y) \\ &+H_y^{c(1)}(M_5^z) + H_y^{c(1)}(M_5^y) = 0 \end{aligned} \tag{2}$$

$$\begin{aligned} &-H_x^{c(1)}(M_1^x) - H_x^{c(1)}(M_1^y) + H_x^{c(1)}(M_2^x) + H_x^{c(2)}(M_2^x) + H_x^{c(1)}(M_2^y) \\ &+H_x^{c(2)}(M_2^y) - H_x^{c(2)}(M_3^x) - H_x^{c(2)}(M_3^y) - H_x^{c(1)}(M_5^z) - H_x^{c(1)}(M_5^y) \\ &+H_x^{c(2)}(M_6^z) + H_x^{c(2)}(M_6^y) - H_x^{c(2)}(M_8^x) - H_x^{c(2)}(M_8^z) = 0 \end{aligned} \tag{3}$$

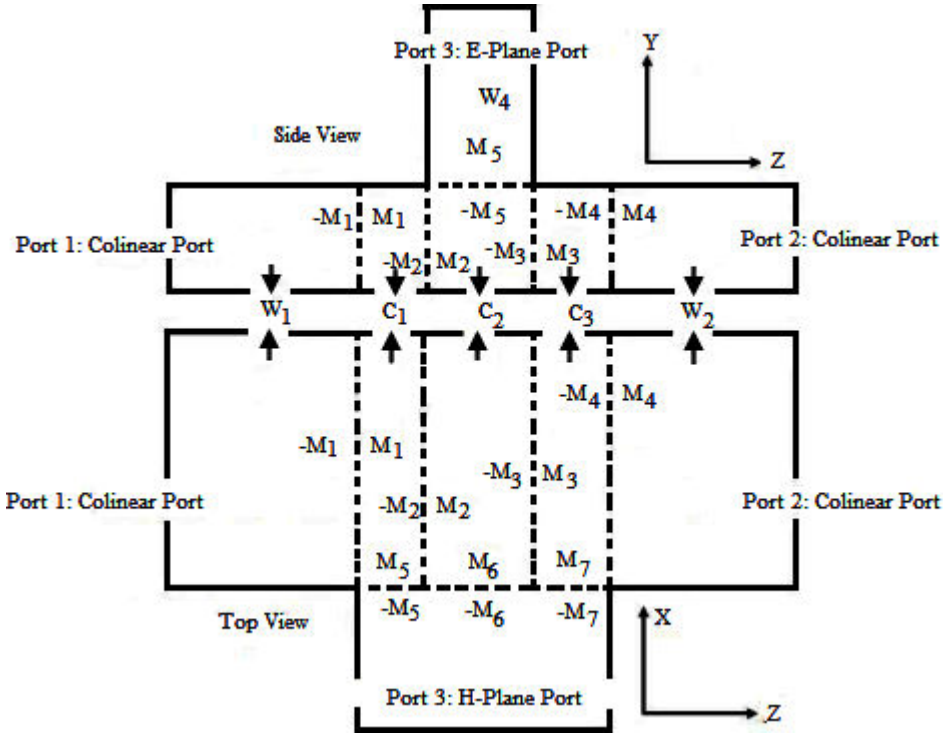

Figure 2. Cavity modeling of the structure with magnetic current at the apertures.

$$\begin{aligned}&-H_y^{c(1)}\left(M_1^x\right)-H_y^{c(1)}\left(M_1^y\right)+H_y^{c(1)}\left(M_2^x\right)+H_y^{c(2)}\left(M_2^x\right)+H_y^{c(1)}\left(M_2^y\right)\\&+H_y^{c(2)}\left(M_2^y\right)-H_y^{c(2)}\left(M_3^x\right)-H_y^{c(2)}\left(M_3^y\right)-H_y^{c(1)}\left(M_5^z\right)-H_y^{c(1)}\left(M_5^y\right)\\&+H_y^{c(2)}\left(M_6^z\right)+H_y^{c(2)}\left(M_6^y\right)-H_y^{c(2)}\left(M_8^x\right)-H_y^{c(2)}\left(M_8^z\right)=0\end{aligned} \tag{4}$$

$$\begin{aligned}&-H_x^{c(2)}\left(M_2^x\right)-H_x^{c(2)}\left(M_2^y\right)+H_x^{c(2)}\left(M_3^x\right)+H_x^{c(3)}\left(M_3^x\right)+H_x^{c(2)}\left(M_3^y\right)\\&+H_x^{c(3)}\left(M_3^y\right)-H_x^{c(3)}\left(M_4^x\right)-H_x^{c(3)}\left(M_4^y\right)-H_x^{c(2)}\left(M_6^z\right)-H_x^{c(2)}\left(M_6^y\right)\\&+H_x^{c(3)}\left(M_7^z\right)+H_x^{c(3)}\left(M_7^y\right)+H_x^{c(2)}\left(M_8^x\right)+H_x^{c(2)}\left(M_8^z\right)=0\end{aligned} \tag{5}$$

$$\begin{aligned}&-H_y^{c(2)}\left(M_2^x\right)-H_y^{c(2)}\left(M_2^y\right)+H_y^{c(2)}\left(M_3^x\right)+H_y^{c(3)}\left(M_3^x\right)+H_y^{c(2)}\left(M_3^y\right)\\&+H_y^{c(3)}\left(M_3^y\right)-H_y^{c(3)}\left(M_4^x\right)-H_y^{c(3)}\left(M_4^y\right)-H_y^{c(2)}\left(M_6^z\right)-H_y^{c(2)}\left(M_6^y\right)\\&+H_y^{c(3)}\left(M_7^z\right)+H_y^{c(3)}\left(M_7^y\right)+H_y^{c(2)}\left(M_8^x\right)+H_y^{c(2)}\left(M_8^z\right)=0\end{aligned} \tag{6}$$

$$\begin{aligned}&-H_x^{c(3)}\left(M_3^x\right)-H_x^{c(3)}\left(M_3^y\right)+H_x^{c(3)}\left(M_4^x\right)+H_x^{w(2)}\left(M_4^x\right)+H_x^{c(3)}\left(M_4^y\right)+H_x^{w(2)}\left(M_4^y\right)\\&-H_x^{c(3)}\left(M_7^z\right)-H_x^{c(3)}\left(M_7^y\right)=2H_x^{inc(2)}\end{aligned} \tag{7}$$

$$\begin{aligned}&-H_y^{c(3)}\left(M_3^x\right)-H_y^{c(3)}\left(M_3^y\right)+H_y^{c(3)}\left(M_4^x\right)+H_y^{w(2)}\left(M_4^x\right)+H_y^{c(3)}\left(M_4^y\right)+H_y^{w(2)}\left(M_4^y\right)\\&-H_y^{c(3)}\left(M_7^z\right)-H_y^{c(3)}\left(M_7^y\right)=0\end{aligned} \tag{8}$$

$$H_z^{c(1)}(M_1^x)+H_z^{c(1)}(M_1^y)-H_z^{c(1)}(M_2^x)-H_z^{c(1)}(M_2^y)+H_z^{c(1)}(M_5^z)$$
$$+H_z^{w(3)}(M_5^z)+H_z^{c(1)}(M_5^y)+H_z^{w(3)}(M_5^y)+H_z^{w(3)}(M_6^z)+H_z^{w(3)}(M_6^y) \tag{9}$$
$$+H_z^{w(3)}(M_7^z)+H_z^{w(3)}(M_7^y)=2H_z^{inc(3)}$$

$$H_y^{c(1)}(M_1^x)+H_y^{c(1)}(M_1^y)-H_y^{c(1)}(M_2^x)-H_y^{c(1)}(M_2^y)+H_y^{c(1)}(M_5^z)+H_y^{w(3)}(M_5^z) \tag{10}$$
$$+H_y^{c(1)}(M_5^y)+H_y^{w(3)}(M_5^y)+H_y^{w(3)}(M_6^z)+H_y^{w(3)}(M_6^y)+H_y^{w(3)}(M_7^z)+H_y^{w(3)}(M_7^y)=0$$

$$H_z^{c(2)}(M_2^x)+H_z^{c(2)}(M_2^y)-H_z^{c(2)}(M_3^x)-H_z^{c(2)}(M_3^y)+H_z^{w(3)}(M_5^z)+H_z^{w(3)}$$
$$(M_5^y)+H_z^{c(2)}(M_6^z)+H_z^{w(3)}(M_6^z)+H_z^{c(2)}(M_6^y)+H_z^{w(3)}(M_6^y)+H_z^{w(3)} \tag{11}$$
$$(M_7^z)+H_z^{w(3)}(M_7^y)-H_z^{c(2)}(M_8^x)-H_z^{c(2)}(M_8^z)=2H_z^{inc(3)}$$

$$H_y^{c(2)}(M_2^x)+H_y^{c(2)}(M_2^y)-H_y^{c(2)}(M_3^x)-H_y^{c(2)}(M_3^y)+H_y^{w(3)}(M_5^y)+H_y^{w(3)}$$
$$(M_5^z)+H_y^{c(2)}(M_6^z)+H_y^{w(3)}(M_6^z)+H_y^{c(2)}(M_6^y)+H_y^{w(3)}(M_6^y)+H_y^{w(3)}(M_7^z) \tag{12}$$
$$+H_y^{w(3)}(M_7^y)-H_y^{c(2)}(M_8^x)-H_y^{c(2)}(M_8^z)=0$$

$$H_z^{c(3)}(M_3^x)+H_z^{c(3)}(M_3^y)-H_z^{c(3)}(M_4^x)-H_z^{c(3)}(M_4^y)+H_z^{w(3)}(M_5^z)$$
$$+H_z^{w(3)}(M_5^y)+H_z^{w(3)}(M_6^z)+H_z^{w(3)}(M_6^y)+H_z^{c(3)}(M_7^z)+H_z^{w(3)}(M_7^z) \tag{13}$$
$$+H_z^{c(3)}(M_7^y)+H_z^{w(3)}(M_7^y)=2H_z^{inc3}$$

$$H_y^{c(3)}(M_3^x)+H_y^{c(3)}(M_3^y)-H_y^{c(3)}(M_4^x)-H_y^{c(3)}(M_4^y)+H_y^{w(3)}(M_5^z)+H_y^{w(3)}(M_5^y) \tag{14}$$
$$+H_y^{w(3)}(M_6^z)+H_y^{w(3)}(M_6^y)+H_y^{c(3)}(M_7^z)+H_y^{w(3)}(M_7^z)+H_y^{c(3)}(M_7^y)+H_y^{w(3)}(M_7^y)=0$$

$$-H_x^{c(2)}(M_2^x)-H_x^{c(2)}(M_2^y)+H_x^{c(2)}(M_3^x)+H_x^{c(2)}(M_3^y)+H_x^{c(3)}(M_3^y)-H_x^{c(2)}(M_6^z) \tag{15}$$
$$-H_x^{c(2)}(M_6^y)+H_x^{c(2)}(M_8^x)+H_x^{w(4)}(M_8^x)+H_x^{c(2)}(M_8^z)+H_x^{w(4)}(M_8^z)=2H_x^{inc(4)}$$

$$-H_z^{c(2)}(M_2^x)-H_z^{c(2)}(M_2^y)+H_z^{c(2)}(M_3^x)+H_z^{c(2)}(M_3^y)+H_z^{c(3)}(M_3^y)-H_z^{c(2)}(M_6^z) \tag{16}$$
$$-H_z^{c(2)}(M_6^y)+H_z^{c(2)}(M_8^x)+H_z^{w(4)}(M_8^x)+H_z^{c(2)}(M_8^z)+H_z^{w(4)}(M_8^z)=0$$

Here:

$$M_i^{\xi/\zeta}=\sum_{p,q=1}^{N}E_{p,q}^{i,\xi/\zeta}T_p(\xi)\,T_q(\zeta)\ \text{where}\begin{cases}\xi=x,\zeta=y\,\text{for aperture}\,1-4\\ \xi=z,\zeta=y\,\text{for aperture}\,5-7\\ \xi=x,\zeta=z\,\text{for aperture}\,8\end{cases} \tag{17}$$

$$T_u(\kappa)=\begin{cases}\frac{\kappa-\kappa_{u-1}}{\kappa_u-\kappa_{u-1}} & \text{for } \kappa_{u-1}\le\kappa\le\kappa_u\\ \frac{\kappa_{u+1}-\kappa}{\kappa_{u+1}-\kappa_u} & \text{for } \kappa_u\le\kappa\le\kappa_{u+1}\end{cases}\quad u=p/q \text{ and } \kappa=\xi/\zeta \tag{18}$$

Expressions of different tangential magnetic field components, mentioned in Eqs. (1)–(16), are as follows:

Incident field:

$$H_{\xi}^{inc(i)} = \begin{cases} -Y_0 \cos\left(\frac{\pi\xi}{2a}\right) e^{-j\beta\chi} \text{ if excited at port "}i\text{"} \\ 0 \qquad\qquad\qquad \text{Otherwise} \end{cases} \quad \text{where} \begin{cases} \xi = x, \chi = z \text{ for } i = 1/2 \\ \xi = z, \chi = x \text{ for } i = 3 \\ \xi = x, \chi = y \text{ for } i = 4 \end{cases} \tag{19}$$

Waveguide field:

$$H_{\xi}^{w(i)}\left(M_i^{\xi}\right) = -\sum_{m=1}^{\infty}\sum_{n=0}^{\infty}\left\{Y_{mn}^{e}\left(C_{mn}^{e}\frac{m\pi}{2a}\right)^2 + Y_{mn}^{m}\left(C_{mn}^{m}\frac{n\pi}{2b}\right)^2\right\}\sin\left\{\frac{m\pi}{2a}(\xi+a)\right\} \cos\left\{\frac{n\pi}{2b}(\zeta+b)\right\} TRIA\xi\xi(p,m)\, TRIA\xi\zeta(q,n) \tag{20}$$

$$H_{\xi}^{w(i)}\left(M_i^{\zeta}\right) = -\sum_{m=0}^{\infty}\sum_{n=1}^{\infty}\left\{Y_{mn}^{e}\left(C_{mn}^{e}\right)^2 - Y_{mn}^{m}\left(C_{mn}^{m}\right)^2\right\}\frac{m\pi}{2a}\frac{n\pi}{2b} \sin\left\{\frac{m\pi}{2a}(\xi+a)\right\}\cos\left\{\frac{n\pi}{2b}(\zeta+b)\right\} TRIA\zeta\xi(p,m)\, TRIA\zeta\zeta(q,n) \tag{21}$$

$$H_{\zeta}^{w(i)}\left(M_i^{\xi}\right) = -\sum_{m=1}^{\infty}\sum_{n=0}^{\infty}\left\{Y_{mn}^{e}\left(C_{mn}^{e}\right)^2 - Y_{mn}^{m}\left(C_{mn}^{m}\right)^2\right\}\frac{m\pi}{2a}\frac{n\pi}{2b} \cos\left\{\frac{m\pi}{2a}(\xi+a)\right\}\sin\left\{\frac{n\pi}{2b}(\zeta+b)\right\} TRIA\xi\xi(p,m)\, TRIA\xi\zeta(q,n) \tag{22}$$

$$H_{\zeta}^{w(i)}\left(M_i^{\zeta}\right) = -\sum_{m=0}^{\infty}\sum_{n=1}^{\infty}\left\{Y_{mn}^{e}\left(C_{mn}^{e}\frac{n\pi}{2b}\right)^2 + Y_{mn}^{m}\left(C_{mn}^{m}\frac{m\pi}{2a}\right)^2\right\} \cos\left\{\frac{m\pi}{2a}(\xi+a)\right\}\sin\left\{\frac{n\pi}{2b}(\zeta+b)\right\} TRIA\zeta\xi(p,m)\, TRIA\zeta\zeta(q,n) \tag{23}$$

Here, $\begin{cases} \xi = x, \zeta = y \text{ for } i = 1/2 \\ \xi = z, \zeta = y \text{ for } i = 3 \\ \xi = x, \zeta = z \text{ for } i = 4 \end{cases}$

$$TRIA\xi\xi(p,m) = \int_{\xi_{i-1}}^{\xi_{i+1}} \sin\left\{\frac{m\pi}{2l_{\xi}}(\xi+a)\right\} T_p(\xi)\, d\xi \;\; (l_{\xi} = a \text{ for } waveguide) \tag{24}$$

$$TRIA\zeta\xi(p,m) = \int_{\xi_{i-1}}^{\xi_{i+1}} \cos\left\{\frac{m\pi}{2l_{\xi}}(\xi+a)\right\} T_p(\xi)\, d\xi \;\; (l_{\xi} = a \text{ for } waveguide) \tag{25}$$

$$TRIA\xi\zeta(q,n) = \int_{\zeta_{i-1}}^{\zeta_{i+1}} \cos\left\{\frac{n\pi}{2l_{\zeta}}(\zeta+l_{\zeta})\right\} T_q(\zeta)\, d\zeta \;\; (l_{\zeta} = b \text{ for waveguide}) \tag{26}$$

$$TRIA\zeta\zeta(q,n) = \int_{\zeta_{i-1}}^{\zeta_{i+1}} \sin\left\{\frac{n\pi}{2l_{\zeta}}(\zeta+l_{\zeta})\right\} T_q(\zeta)\, d\zeta \;\; (l_{\zeta} = b \text{ for waveguide}) \tag{27}$$

Cavity fields:

$$H_{\xi}^{c(i)}\left(M_i^{\xi}\right)=\frac{j\omega\varepsilon}{k^2}\sum_{m=1}^{\infty}\sum_{n=0}^{\infty}\frac{\varepsilon_m\varepsilon_n}{4l_{\xi}l_{\zeta}}\left\{k^2-\left(\frac{m\pi}{2l_{\xi}}\right)^2\right\}\sin\left\{\frac{m\pi}{2l_{\xi}}\left(\xi+l_{\xi}\right)\right\}\cos\left\{\frac{n\pi}{2l_{\zeta}}\left(\zeta+l_{\zeta}\right)\right\}$$
$$\frac{TRIA\xi\xi(p,m)TRIA\xi\zeta(q,n)}{\Gamma_{mn\chi}\sin(2\Gamma_{mn\chi}\chi)}\begin{cases}\cos\left\{\Gamma_{mn\chi}\left(\chi-l_{\chi}\right)\right\}\cos\left\{\Gamma_{mn\chi}\left(\chi'+l_{\chi}\right)\right\} & \text{for } \chi>\chi'\\ \cos\left\{\Gamma_{mn\chi}\left(\chi'-l_{\chi}\right)\right\}\cos\left\{\Gamma_{mn\chi}\left(\chi+l_{\chi}\right)\right\} & \text{for } \chi<\chi'\end{cases} \tag{28}$$

$$H_{\xi}^{c(i)}\left(M_i^{\zeta}\right)=-\frac{j\omega\varepsilon}{k^2}\sum_{m=0}^{\infty}\sum_{n=1}^{\infty}\frac{\varepsilon_m\varepsilon_n}{4l_{\xi}l_{\zeta}}\frac{m\pi}{2l_{\xi}}\frac{n\pi}{2l_{\zeta}}\sin\left\{\frac{m\pi}{2l_{\xi}}\left(\xi+l_{\xi}\right)\right\}\cos\left\{\frac{n\pi}{2l_{\zeta}}\left(\zeta+l_{\zeta}\right)\right\}$$
$$\frac{TRIA\zeta\xi(p,m)TRIA\zeta\zeta(q,n)}{\Gamma_{mn\chi}\sin(2\Gamma_{mn\chi}\chi)}\begin{cases}\cos\left\{\Gamma_{mn\chi}\left(\chi-l_{\chi}\right)\right\}\cos\left\{\Gamma_{mn\chi}\left(\chi'+l_{\chi}\right)\right\} & \text{for } \chi>\chi'\\ \cos\left\{\Gamma_{mn\chi}\left(\chi'-l_{\chi}\right)\right\}\cos\left\{\Gamma_{mn\chi}\left(\chi+l_{\chi}\right)\right\} & \text{for } \chi<\chi'\end{cases} \tag{29}$$

$$H_{\zeta}^{c(i)}\left(M_i^{\xi}\right)=-\frac{j\omega\varepsilon}{k^2}\sum_{m=1}^{\infty}\sum_{n=0}^{\infty}\frac{\varepsilon_m\varepsilon_n}{4l_{\xi}l_{\zeta}}\frac{m\pi}{2l_{\xi}}\frac{n\pi}{2l_{\zeta}}\cos\left\{\frac{m\pi}{2l_{\xi}}\left(\xi+l_{\xi}\right)\right\}\sin\left\{\frac{n\pi}{2l_{\zeta}}\left(\zeta+l_{\zeta}\right)\right\}$$
$$\frac{TRIA\xi\xi(p,m)TRIA\xi\zeta(q,n)}{\Gamma_{mn\chi}\sin(2\Gamma_{mn\chi}\chi)}\begin{cases}\cos\left\{\Gamma_{mn\chi}\left(\chi-l_{\chi}\right)\right\}\cos\left\{\Gamma_{mn\chi}\left(\chi'+l_{\chi}\right)\right\} & \text{for } \chi>\chi'\\ \cos\left\{\Gamma_{mn\chi}\left(\chi'-l_{\chi}\right)\right\}\cos\left\{\Gamma_{mn\chi}\left(\chi+l_{\chi}\right)\right\} & \text{for } \chi<\chi'\end{cases} \tag{30}$$

$$H_{\zeta}^{c(i)}\left(M_i^{\zeta}\right)=\frac{j\omega\varepsilon}{k^2}\sum_{m=0}^{\infty}\sum_{n=1}^{\infty}\frac{\varepsilon_m\varepsilon_n}{4l_{\xi}l_{\zeta}}\left\{k^2-\left(\frac{n\pi}{2l_{\zeta}}\right)^2\right\}\cos\left\{\frac{m\pi}{2l_{\xi}}\left(\xi+l_{\xi}\right)\right\}\sin\left\{\frac{n\pi}{2l_{\zeta}}\left(\zeta+l_{\zeta}\right)\right\}$$
$$\frac{TRIA\zeta\xi(p,m)TRIA\zeta\zeta(q,n)}{\Gamma_{mn\chi}\sin(2\Gamma_{mn\chi}\chi)}\begin{cases}\cos\left\{\Gamma_{mn\chi}\left(\chi-l_{\chi}\right)\right\}\cos\left\{\Gamma_{mn\chi}\left(\chi'+l_{\chi}\right)\right\} & \text{for } \chi>\chi'\\ \cos\left\{\Gamma_{mn\chi}\left(\chi'-l_{\chi}\right)\right\}\cos\left\{\Gamma_{mn\chi}\left(\chi+l_{\chi}\right)\right\} & \text{for } \chi<\chi'\end{cases} \tag{31}$$

$$H_{\chi}^{c(i)}\left(M_i^{\xi}\right)=-\frac{j\omega\varepsilon}{k^2}\sum_{m=1}^{\infty}\sum_{n=0}^{\infty}\frac{\varepsilon_m\varepsilon_n}{4l_{\xi}l_{\zeta}}\frac{m\pi}{2l_{\xi}}\cos\left\{\frac{m\pi}{2l_{\xi}}\left(\xi+l_{\xi}\right)\right\}\cos\left\{\frac{n\pi}{2l_{\zeta}}\left(\zeta+l_{\zeta}\right)\right\}$$
$$\frac{TRIA\xi\xi(p,m)TRIA\xi\zeta(q,n)}{\sin(2\Gamma_{mn\chi}\chi)}\begin{cases}\sin\left\{\Gamma_{mn\chi}\left(\chi-l_{\chi}\right)\right\}\cos\left\{\Gamma_{mn\chi}\left(\chi'+l_{\chi}\right)\right\} & \text{for } \chi>\chi'\\ \cos\left\{\Gamma_{mn\chi}\left(\chi'-l_{\chi}\right)\right\}\sin\left\{\Gamma_{mn\chi}\left(\chi+l_{\chi}\right)\right\} & \text{for } \chi<\chi'\end{cases} \tag{32}$$

$$H_{\chi}^{c(i)}\left(M_i^{\zeta}\right)=-\frac{j\omega\varepsilon}{k^2}\sum_{m=0}^{\infty}\sum_{n=1}^{\infty}\frac{\varepsilon_m\varepsilon_n}{4l_{\xi}l_{\zeta}}\frac{n\pi}{2l_{\zeta}}\cos\left\{\frac{m\pi}{2l_{\xi}}\left(\xi+l_{\xi}\right)\right\}\cos\left\{\frac{n\pi}{2l_{\zeta}}\left(\zeta+l_{\zeta}\right)\right\}$$
$$\frac{TRIA\zeta\xi(p,m)TRIA\zeta\zeta(q,n)}{\sin(2\Gamma_{mn\chi}\chi)}\begin{cases}\sin\left\{\Gamma_{mn\chi}\left(\chi-l_{\chi}\right)\right\}\cos\left\{\Gamma_{mn\chi}\left(\chi'+l_{\chi}\right)\right\} & \text{for } \chi>\chi'\\ \cos\left\{\Gamma_{mn\chi}\left(\chi'-l_{\chi}\right)\right\}\sin\left\{\Gamma_{mn\chi}\left(\chi+l_{\chi}\right)\right\} & \text{for } \chi<\chi'\end{cases} \tag{33}$$

$(2l_{\xi},2l_{\zeta},2l_{\chi})$ are dimensions of the cavity along the (ξ,ζ,χ) direction, where: $(\xi,\zeta,\chi)=\begin{cases}(x,y,z) & \text{for } i=1\,to\,4\\ (z,y,x) & \text{for } i=5\,to\,7\\ (x,z,y) & \text{for } i=8\end{cases}$

To solve the boundary conditions in Eqs. (1)–(16), Galerkin's specialization of the method of moment has been used, where the weighting function is considered as follows.

$$W_i^{\xi}=\sum_{p,q=1}^{N}T_p\left(\xi\right)T_q\left(\zeta\right)\text{ where }\begin{cases}\xi=x,\zeta=y\,\text{for aperture}\,1-4\\ \xi=z,\zeta=y\,\text{for aperture}\,5-7\\ \xi=x,\zeta=z\,\text{for aperture}\,8\end{cases} \tag{34}$$

The S-parameters can be found using the following relations.

$$S_{11} = -1 + \frac{1}{2ab} \sum_{p,q=1}^{N} E_{p,q}^{1,x} TRIAXX(p,1) TRIAXY(q,0) \tag{35}$$

$$S_{21} = \frac{1}{2ab} \sum_{p,q=1}^{N} E_{p,q}^{4,x} TRIAXX(p,1) TRIAXY(q,0) \tag{36}$$

$$S_{13} = \frac{1}{2ab} \sum_{p,q=1}^{N} E_{p,q}^{1,x} TRIAXX(p,1) TRIAXY(q,0) \tag{37}$$

$$\begin{aligned} S_{33} = -1 + \tfrac{1}{2ab} \Bigg\{ & \sum_{p,q=1}^{N} E_{p,q}^{5,z} TRIAZZ(p,1) TRIAZY(q,0) + \sum_{p,q=1}^{N} E_{p,q}^{6,z} TRIAZZ(p,1) \\ & TRIAZY(q,0) + \sum_{p,q=1}^{N} E_{p,q}^{7,z} TRIAZZ(p,1) TRIAZY(q,0) \Bigg\} \end{aligned} \tag{38}$$

$$S_{14} = \frac{1}{2ab} \sum_{p,q=1}^{N} E_{p,q}^{1,x} TRIAXX(p,1) TRIAXY(q,0) \tag{39}$$

$$S_{44} = -1 + \frac{1}{2ab} \sum_{p,q=1}^{N} E_{p,q}^{8,x} TRIAXX(p,1) TRIAXY(q,0) \tag{40}$$

The rest of the S-parameters are symmetric.

The frequency responses of the magnitude of scattering parameters of the network are found using Eqs. (35)–(40) and are plotted in Figure 3. Frequency responses of the magnitude of the scattering parameters of the network, obtained using CST Microwave Studio simulation, are also plotted in the same figure for validation of the analysis. All the responses are in excellent agreement, which validates the analysis.

3. Design of matched E-H plane T-junction

The frequency responses of the network, shown in Figure 3, reveal that the ports are unmatched. In order to establish simultaneous matching at all the ports a matching network has been included, as shown in Figure 4. When the network is excited at any of its ports a current is induced on the matching network, which, in turn, produces a scattered field. The scattered field cancels the reflected field from the junction and thus improves the matching. Parametric analysis of the network has been carried out using CST Microwave Studio version 14 and the results are shown in Figures 5–11. The optimized dimensions of different geometrical parameters of the matching network and their effects on the frequency response of the network are tabulated in Table 1.

The above parametric studies of the matched E-H plane T-junction reveal that the bisected funnel structure mainly matches the E-plane arm without affecting the matching of the collinear and H-plane arms much, whereas the iris structure mainly matches the collinear and H-plane arms without affecting the matching of the E-plane arm much. The independent matching characteristics of the matching network makes the simultaneous matching of the overall network much easier and faster.

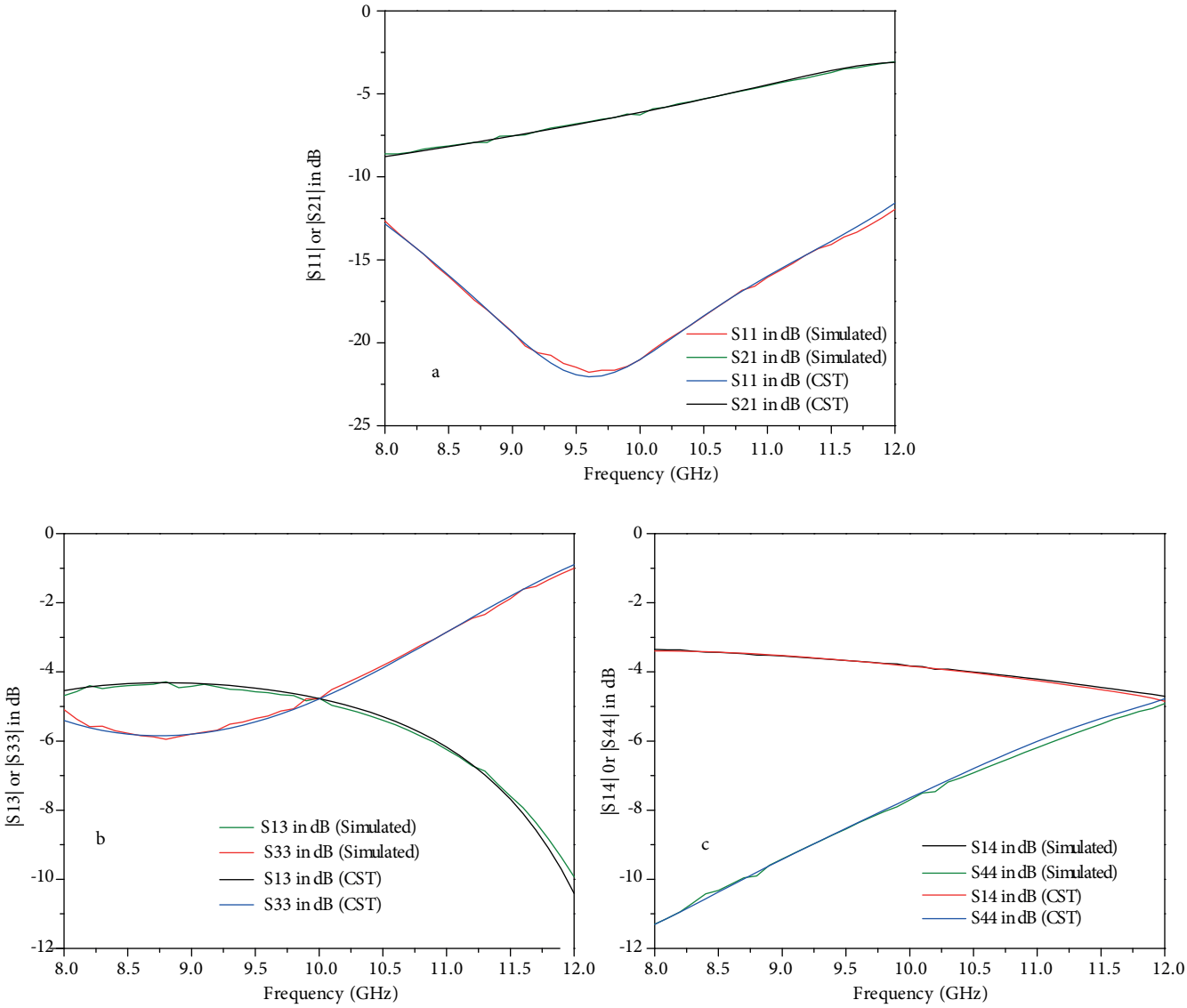

Figure 3. Comparisons of the frequency responses of an E-H plane T-junction obtained using the proposed method and CST Microwave Studio simulation for (a) $|S_{11}|$ and $|S_{21}|$, (b) $|S_{13}|$ and $|S_{33}|$, (c) $|S_{14}|$ and $|S_{44}|$.

In order to design a matched E-H plane T-junction at an arbitrary design frequency one needs to optimize the different geometrical parameters of the matching networks. Table 1 reveals that out of the different geometrical parameters, d, xs, rbc, rtc, and ch decide the matching frequency whereas the rest of the parameters improve the magnitude of matching. In order to estimate the initial values of these parameters, Figure 5–11 may be revisited. The observations are summarized in Table 2. The table reveals that to design a matching network at an arbitrary frequency the following dimensions may be taken as the initial values for optimization: d $\approx 0.1\lambda_g$, xs $\approx 0.3\lambda_g$, rbc $\approx 0.45\lambda_g$, rtc $\approx 0.03\lambda_g$, and ch $\approx 0.17\lambda_g$. Optimized electrical lengths of th and ph are approximately $0.01\lambda_g$ and $0.45\lambda_g$, respectively.

The optimized frequency responses of the matched E-H plane T-junction have been plotted in Figure 12 and compared with measured frequency responses of the fabricated matched E-H plane T-junction. The measurements have been carried out using a Keysight N5221A PNA. The responses are in close agreement. Slight

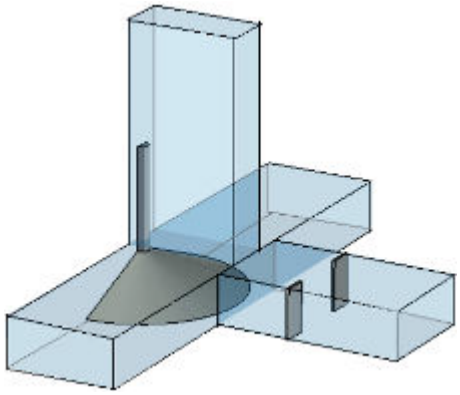

Figure 4. Matched E-H plane T-junction.

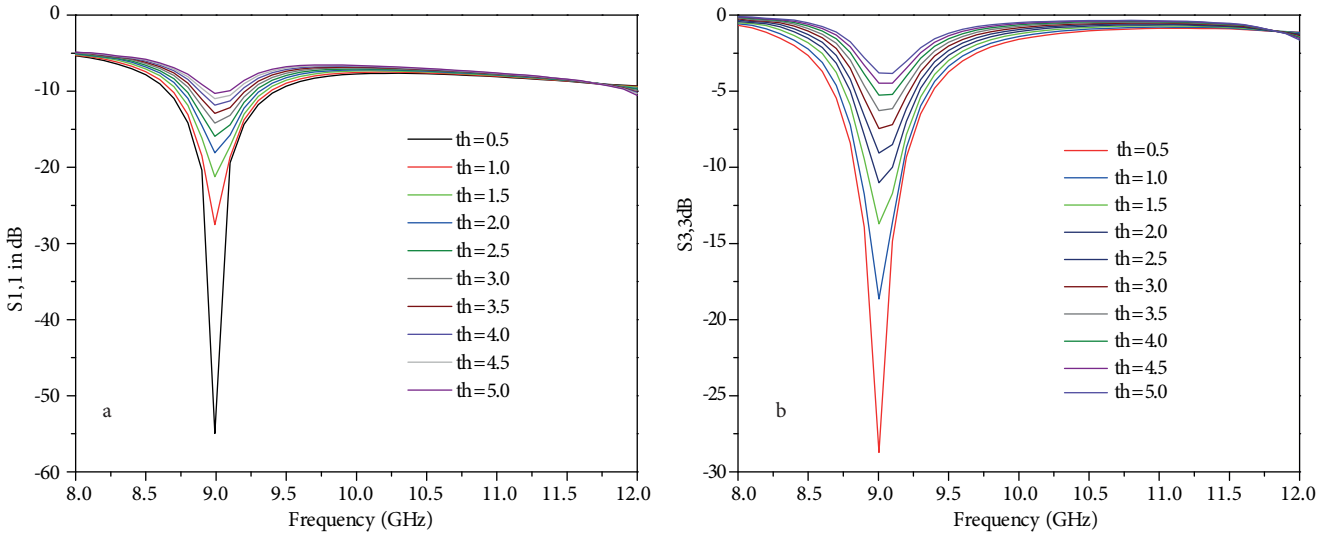

Figure 5. Parametric analysis of the matched E-H plane T-junction for different thicknesses of the iris in H-plane arm (th) for (a) $|S_{11}|$ and (b) $|S_{33}|$.

mismatches between the responses are due to possible fabrication errors, surface roughness of the waveguide and matching stubs, and parasitic effects of the small discontinuities.

4. Conclusion

This paper presents a method of moment-based analysis of an E-H plane T-junction. The analysis shows that the network is not matched at its ports. Therefore, to achieve simultaneous matching at all its ports, a matching network has been incorporated. The matching network consists of a bisected funnel structure at the junction and an iris at the H-plane arm. It has been shown that the bisected funnel structure matches the E-plane arm without affecting the matching of the collinear and H-plane arms much, whereas the iris structure mainly matches the collinear and H-plane arms without affecting the matching of the E-plane arm much. The independent matching characteristics of the two matching networks make simultaneous matching of the overall network much easier and faster. Discussions have also been made on how to estimate the initial values of the different geometrical parameters of the matching network if anyone wants to design an E-H plane T-junction at a different frequency.

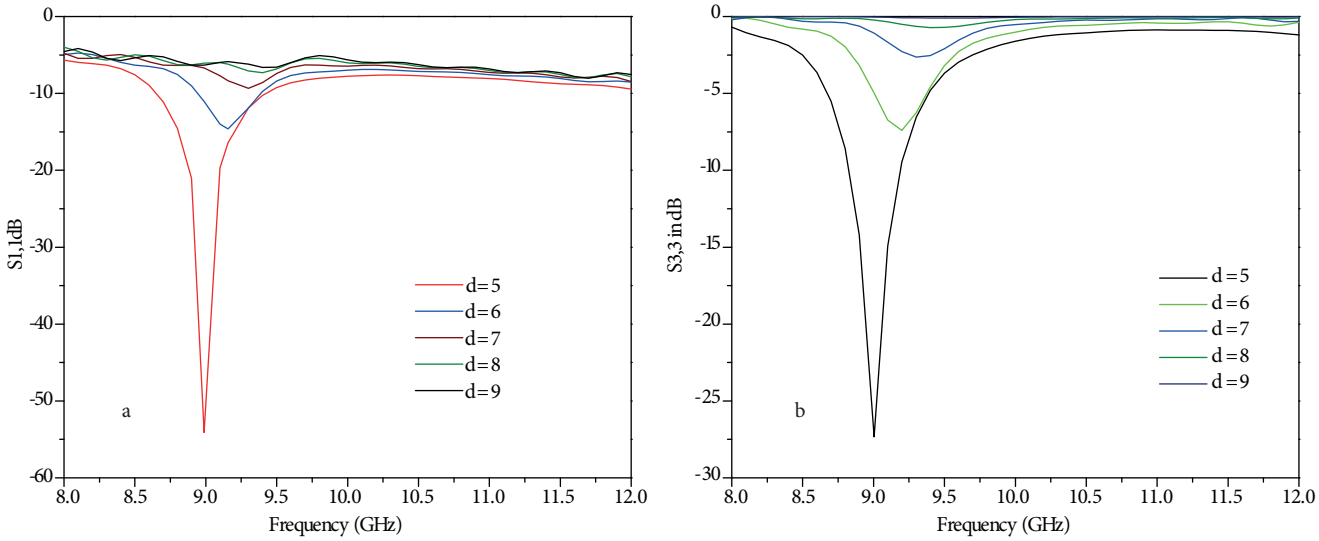

Figure 6. Parametric analysis of the matched E-H plane T-junction for different widths of the iris in H-plane arm (d) for (a) $|S_{11}|$ and (b) $|S_{33}|$.

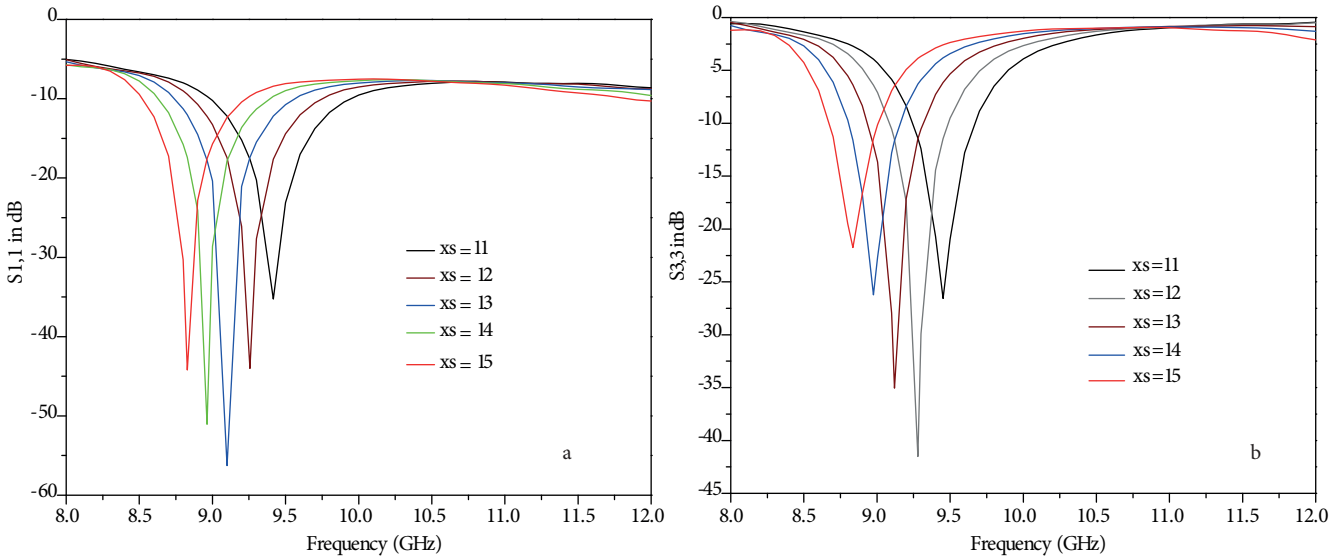

Figure 7. Parametric analysis of the matched E-H plane T-junction for different distances of the iris in H-plane arm from the junction (xs) for (a) $|S_{11}|$ and (b) $|S_{33}|$.

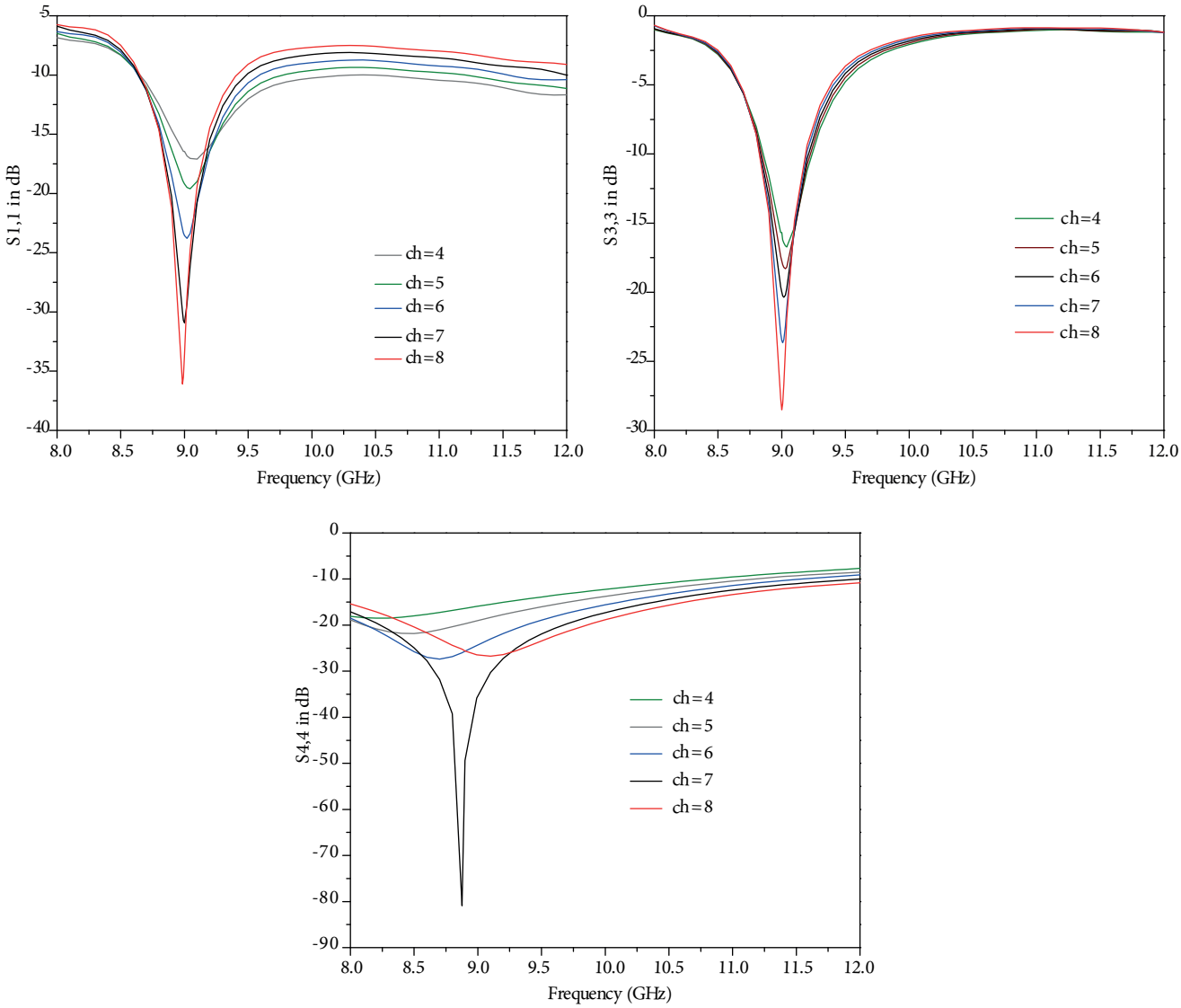

Figure 8. Parametric analysis of the matched E-H plane T-junction for different heights of the cone of the bisected funnel structure (ch) for (a) $|S_{11}|$, (b) $|S_{33}|$, and (b) $|S_{44}|$.

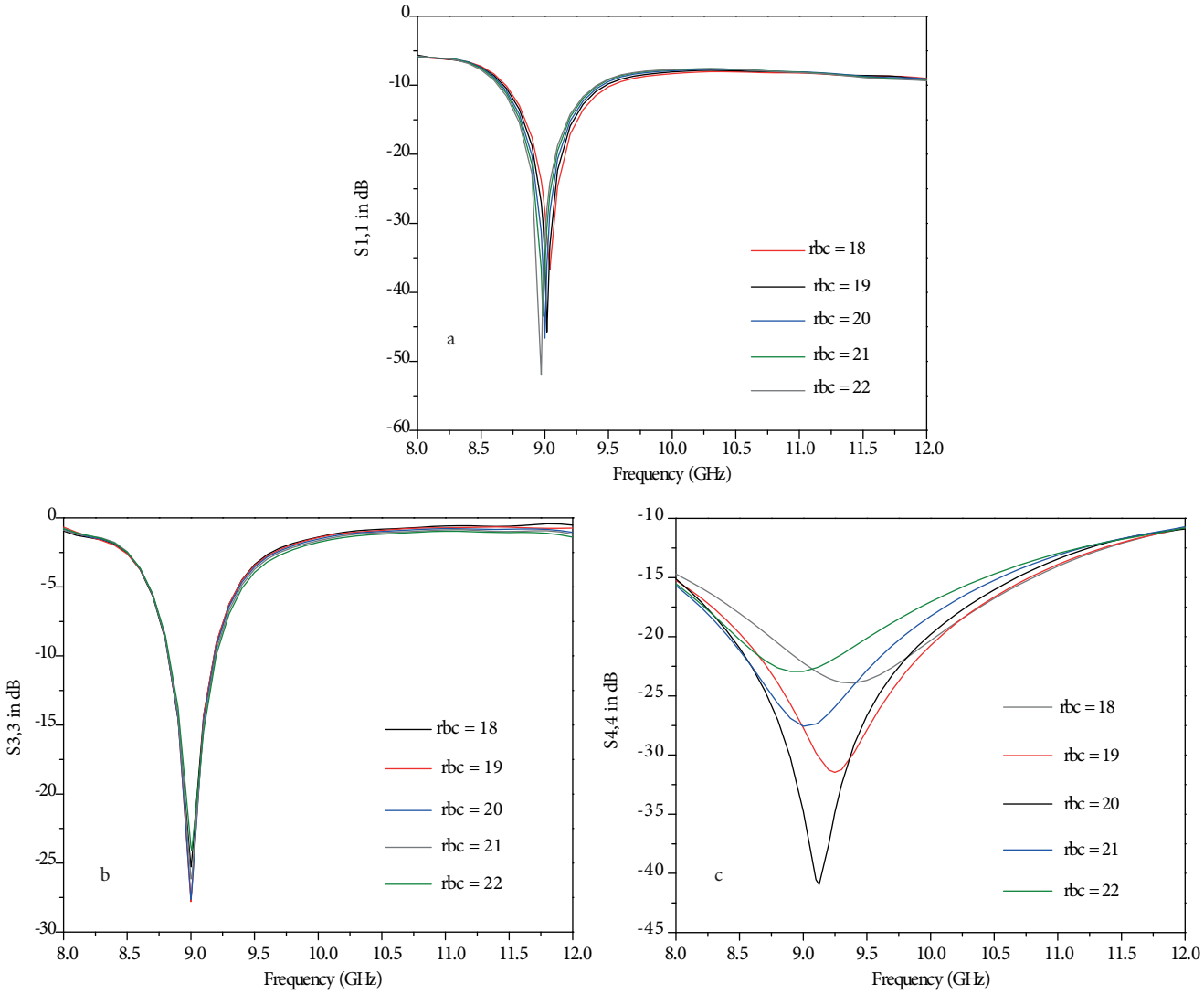

Figure 9. Parametric analysis of the matched E-H plane T-junction for different bottom radii of the cone of the bisected funnel structure (rbc) for (a) $|S_{11}|$, (b) $|S_{33}|$, and (b) $|S_{44}|$.

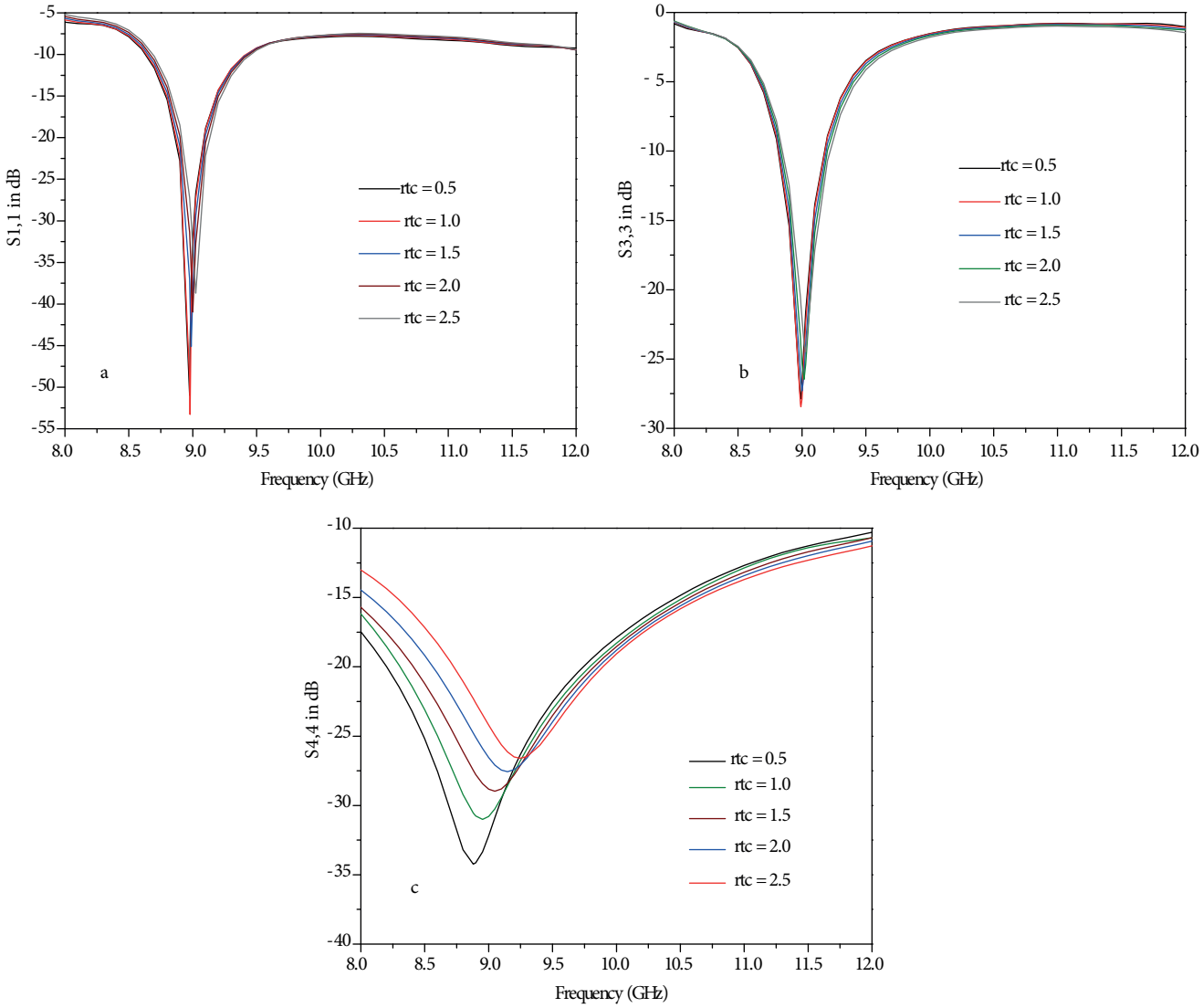

Figure 10. Parametric analysis of the matched E-H plane T-junction for different top radii of the cone of the bisected funnel structure (rtc) for (a) $|S_{11}|$, (b) $|S_{33}|$, and (c) $|S_{44}|$.

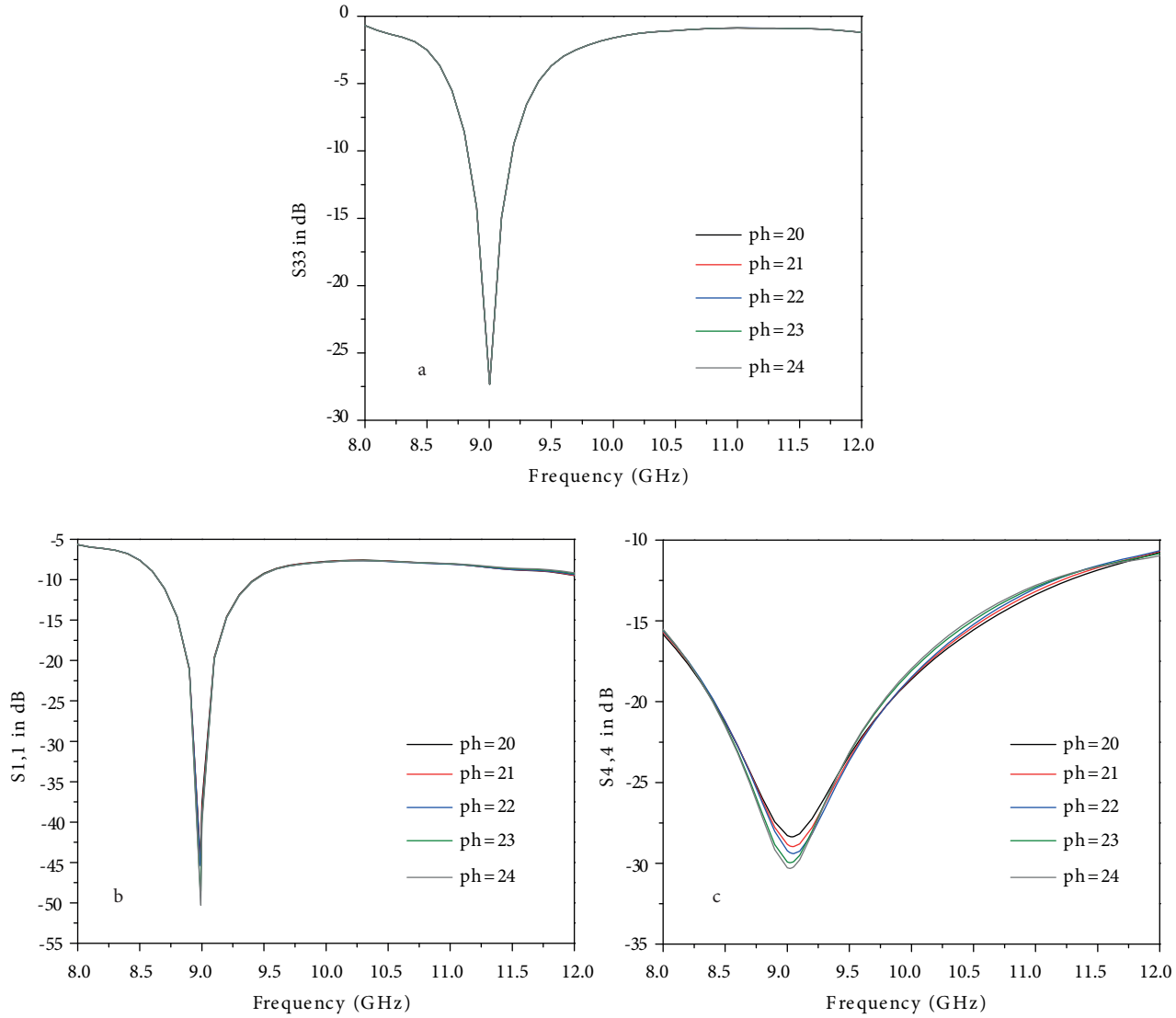

Figure 11. Parametric analysis of the matched E-H plane T-junction for different post heights of the bisected funnel structure (ph) for (a) $|S_{11}|$, (b) $|S_{33}|$, and (b) $|S_{44}|$.

Table 1. Optimized dimensions of the matching network.

Sl. no.	Description of the parameter	Effect on matching (when the value of the parameter is increased)	Optimized dimension
1	Thickness of the iris in H-plane arm (th)	(i) Improves matching at collinear and H-plane arms. (ii) No effect on matching frequency. (iii) No effect on matching of E-plane arm.	0.5 mm
2.	Width of the iris in H-plane arm (d)	(i) Matching at collinear and H-plane arms deteriorates very fast. (ii) Shifts matching frequency at higher frequency. (iii) No effect on matching of E-plane arm.	5.0 mm
3.	Position of the iris from the junction (xs)	(i) Matching at the collinear and H-plane arms deteriorates slowly. (ii) Shifts matching frequency at higher frequency. (iii) No effect on matching of E-plane arm.	13.8 mm
4.	Cone height (ch)	(i) Shifts matching frequency of the E-plane arm towards higher frequency. (ii) The matching of the arm initially improves and then deteriorates. (iii) Improves matching of the collinear and H-plane arms without major changes in the matching frequency.	7.8 mm
5.	Bottom radius of cone (rbc)	(i) Shifts matching frequency of the E-plane arm towards lower frequency. (ii) The matching of the arm initially improves and then deteriorates. (iii) No major effect on matching and matching frequency of the collinear and H-plane arms.	20.8 mm
6.	Top radius of cone (rtc)	(i) Shifts matching frequency of the E-plane arm towards higher frequency. (ii) The matching of the arm deteriorates slowly. (iii) No major effect on matching and matching frequency of the collinear and H-plane arms.	1.5 mm
7.	Height of the post (ph)	(i) Improves the matching of the E-plane arm slowly. (ii) Has no effect on the matching frequency of E-plane arm. (ii) Has no effect on the matching of the collinear and H-plane arms.	21 mm

Table 2. Summary of parametric analysis.

Sl. no.	Parameter	Dimension (mm)	Resonant frequency (GHz)	Electrical length	Optimized elec. length
1	d	5–7	9–9.34	$0.1135\lambda_g$–$0.1653\lambda_g$	$0.1061\lambda_g$
2	xs	11–15	9.45–8.84	$0.2628\lambda_g$–$0.3337\lambda_g$	$0.2922\lambda_g$
3	rbc	18–22	9.37–9.25	$0.3984\lambda_g$–$0.4806\lambda_g$	$0.4438\lambda_g$
4	rtc	0.5–2.5	8.88–9.26	$0.0104\lambda_g$–$0.054\lambda_g$	$0.032\lambda_g$
5	ch	4–8	8.23–9.1	$0.0746\lambda_g$–$0.1718\lambda_g$	$0.1664\lambda_g$

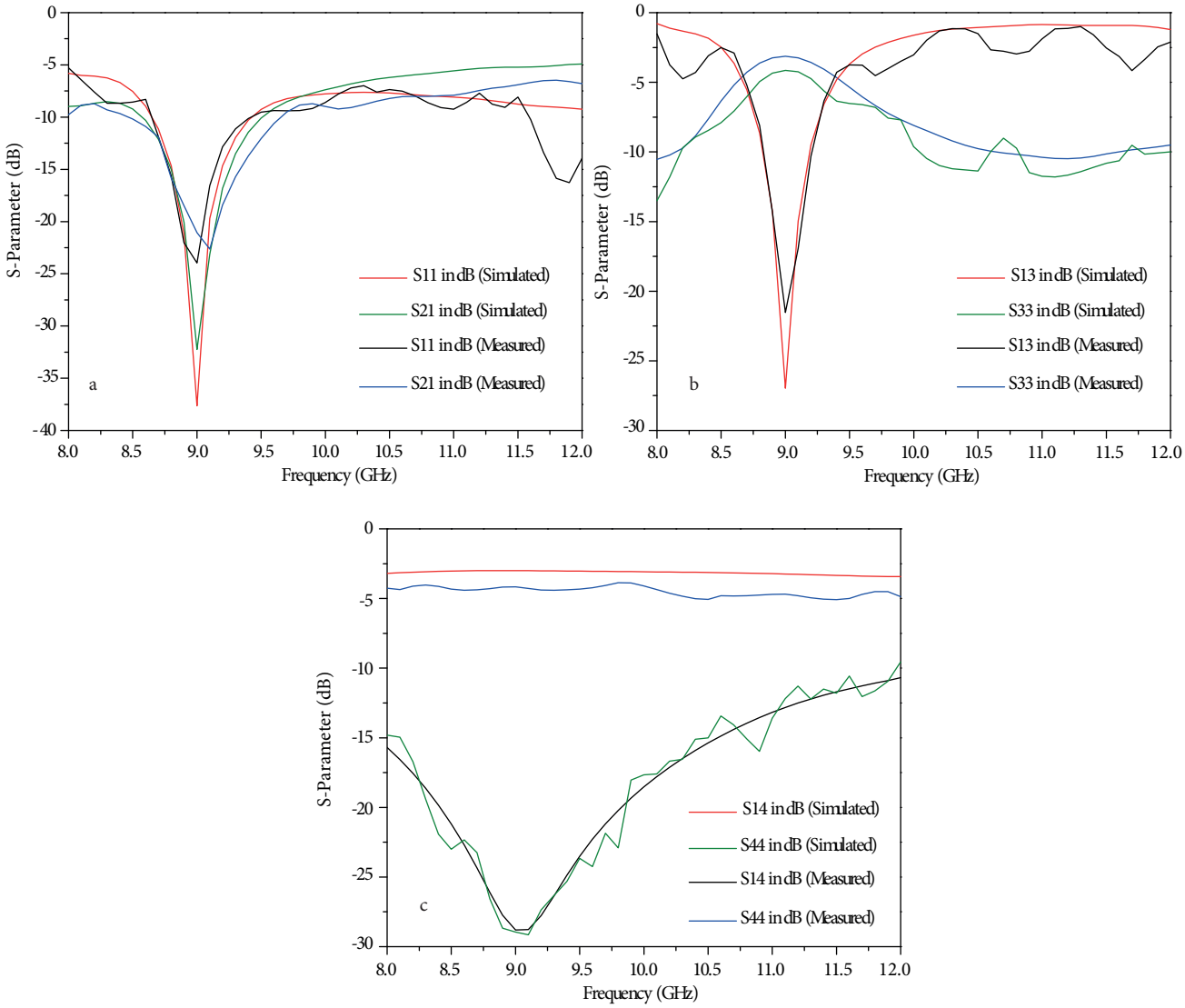

Figure 12. Comparisons of the simulated and measured frequency responses of the matched E-H plane T-junction for (a) $|S_{11}|$ and $|S_{21}|$, (b) $|S_{13}|$ and $|S_{33}|$, (c) $|S_{14}|$ and $|S_{44}|$.

Acknowledgments

The authors would like to thank Dr Sushrut Das, Associate Professor, Department of Electronics Engineering, Indian Institute of Technology (Indian School of Mines), Dhanbad, for his suggestions during this work. The authors are also thankful to the Department of Science and Technology (DST), Government of India, for its support through the FIST Project.

References

[1] Sieverding T, Arndt F. Modal analysis of magic tee. IEEE Microw Guided W 1993; 3: 150-152.

[2] Ritter J, Arndt F. Efficient FDTD/matrix-pencil method for the full-wave scattering parameter analysis of waveguide structure. IEEE T Microw Theory 1996; 44: 2450-2456.

[3] Shen Z, Law CL, Qian C. Hybrid finite-element-model-expansion method for magic T-junction. IEEE T Magn 2002; 38: 385-388.

[4] Beyer R, Rosenberg U. CAD of magic tee with interior stepped post for high performance designs. In: IEEE MTT-S International Microwave Symposium Digest; 8–13 June 2003; Philadelphia, PA, USA. New York, NY, USA: IEEE. pp. 1207-1210.

[5] Dou WB, Zhang YZ. Forked hybrid waveguide T-junctions analyzed by FDTD method. J Electromagnet Wave 2003; 17: 517-523.

[6] Wu HC, Dou WB. A rigorous analysis and experimental researches of waveguide magic tee at W band. Prog Electromagn Res 2006; 60: 131-142.

[7] Das S, Chakraborty A. A novel modeling technique to solve a class of rectangular waveguide based circuits and radiators. Prog Electromagn Res 2006; 61: 231-252.